Supporting Information for: "Probing the Photoinduced Metal–Nitrosyl Linkage Isomerism of Sodium Nitroprusside in Solution Using Transient Infrared Spectroscopy"

Michael S. Lynch, Mark Cheng, Benjamin E. Van Kuiken and Munira Khalil*

Department of Chemistry, University of Washington, Seattle, Washington 98195

Contents

Figures

Tables

* Corresponding author E-mail address: mkhalil@chem.washington.edu

SI. Bleach Dynamics

The metastable nature of the transient species is clear from the bleach recovery dynamics, shown in Figure S1, as there is no recovery evident through 0.5 ns. Fig. S1a shows the NO bleach, where self-absorption (positive dip) is present due to the high sample concentration (120 mM). Note that since the NO stretching frequencies of the transient species are well separated from the NO bleach, the high sample concentration does not have an effect on the dynamics of the transient species. The 32 ± 7 ps vibrational relaxation timescale of ν_{NO} (2 ← 1) is shown in Figure S1b. This timescale is consistent with the population relaxation time (T_1) of ν_{NO} (1 ← 0) in SNP dissolved in methanol reported by Owrutsky and co-workers of 29 ± 2 ps.[1]

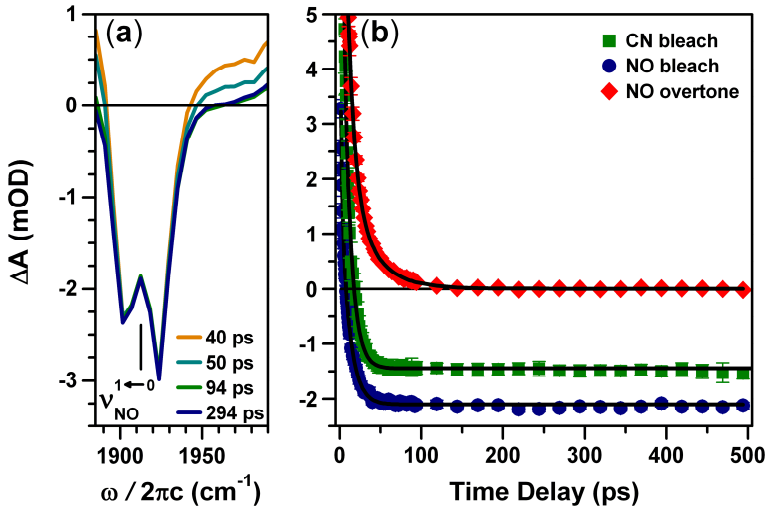

Figure S1. (a) Time-resolved infrared absorption spectra of SNP in methanol at 295 K showing the ν_{NO} bleach at 1909 cm^{-1}. (b) Bleach dynamics of the ν_{NO} (blue circles, 1909 cm^{-1}), ν_{CN} (green squares, 2145 cm^{-1}) and ν_{NO} overtone (red diamonds, 1881 cm^{-1}). Best fits to the data are shown as black solid lines.

SII. Kinetic Parameters Extracted from Best Fit

A. NO stretching region

Table S1 presents the fitting parameters extracted from the NO stretching region of the transient IR spectrum fit to Equation 1. The data for neat methanol is given in Table S2. The neat methanol data illustrates that solvent and/or CaF_2 relaxation dominates the first two decay channels. Each of the kinetic traces was obtained by integrating the spectral resonance over the full-width at half-maximum (FWHM) of the peak to ensure accurate kinetic parameters.

$$\Delta A = \sum_{i=1}^{3} A_i e^{-t/\tau_i} \qquad (1)$$

Table S1. Best-fit parameters for transients in the NO stretching region.

Assignment	ω_c (cm^{-1})	τ_1 (ps)	τ_2 (ps)	τ_3 (ns)	A_1 [b]	A_2	A_3	ΔA_{inf} (mOD) [c]
MS1	1794	2.6 ± 0.5	11.6 ± 0.5	83[a]	0.56 ± 0.06	0.47 ± 0.04	0.011 ± 0.003	–
MS2	1652	2.6 ± 0.5	12.2 ± 0.3	200[a]	0.52 ± 0.06	0.47 ± 0.03	0.011 ± 0.002	–
NO·	1851	3.3 ± 0.6	13.1 ± 0.5	200[a]	0.52 ± 0.04	0.47 ± 0.05	0.007 ± 0.002	–
NO bleach	1909	2.3 ± 0.6	11 ± 1	–	0.44 ± 0.06	0.56 ± 0.05	–	–2.11 ± 0.02
NO overtone	1881	1.8 ± 0.5	9 ± 1	32 ± 7	0.37 ± 0.05	0.52 ± 0.04	0.11 ± 0.05	–

[a] Approximate values due to the maximum time delay of 0.5 ns in this experiment. The bounds of the fit were held between 80–200 ps. [b] Amplitudes normalized such that $\Sigma_i A_i = 1$. [c] A constant offset replaced A_3 for the bleach since it goes negative.

There is a lot of discussion in the article regarding the early-time solvent response (the solvent refers to both methanol and the sample cell windows) as it is this response that hinders the observation of the early photochemical events occurring in this experiment. Figure S2 shows the FTIR spectrum of SNP in methanol (solvent subtracted) and neat methanol to illustrate the non-zero absorbance of the solvent over the entire spectral region of this experiment. This leads to resonant solvent response at early time delays.

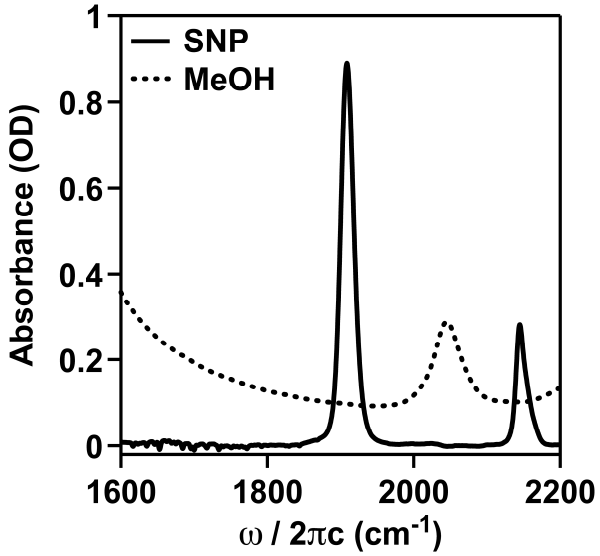

Figure S2. FTIR spectra of 120 mM SNP in methanol (solid line, solvent subtracted) and neat methanol (dotted line) at room temperature with l = 50 μm. The resonance at 2045 cm^{-1} in the neat methanol spectrum is the $2\nu_{CO}$ mode.[2]

Table S2. Best-fit parameters for neat methanol in the NO stretching region.

Assignment	ω_c (cm^{-1})	τ_1 (ps)	τ_2 (ps)	A_1[a]	A_2
MS1	1794	2.3 ± 0.3	11.7 ± 0.5	0.49 ± 0.03	0.51 ± 0.03
MS2	1652	2.4 ± 0.3	11.7 ± 0.5	0.49 ± 0.03	0.51 ± 0.03
NO·	1851	2.2 ± 0.3	11.4 ± 0.5	0.49 ± 0.04	0.51 ± 0.03
NO bleach	1909	2.3 ± 0.2	9.2 ± 0.7	0.68 ± 0.03	0.31 ± 0.03
NO overtone	1881	2.4 ± 0.2	9.4 ± 0.7	0.69 ± 0.03	0.31 ± 0.04

[a] Amplitudes normalized such that $\Sigma_i A_i = 1$.

B. CN stretching region

Table S3 shows the extracted fitting parameters (using Eqn. 2) obtained from the CN stretching region along with assignments consistent with the work of Rest and co-workers.[3] Recall that the stretching frequency of CN^- in methanol was confirmed by taking an FTIR spectrum of 0.25 M KCN in methanol, whereas the Prussian blue stretching frequency was measured in our laboratory using transient IR absorption spectroscopy (i.e. allowing a high concentration of PB to form such that a bleach appears in the transient IR spectrum).

$$\Delta A = \sum_{i=1}^{2} A_i e^{-t/\tau_i} + A_3(1 - e^{-t/\tau_3}) \qquad (2)$$

Table S3. Best-fit parameters for transients in the CN stretching region.

Assignment	ω_c (cm^{-1})	τ_1 (ps)	τ_2 (ps)	τ_3 (ps)	A_1[a]	A_2	A_3	ΔA_{inf} (mOD) [b]
$[Fe^{III}(CN)_5(CH_3OH)]^{2-}$	2123	3.5 ± 0.8	13 ± 1	95 ± 9	0.66 ± 0.07	0.27 ± 0.09	0.070 ± 0.008	–
Prussian blue	2100	3.1 ± 0.8	12 ± 1	40 ± 4	0.65 ± 0.07	0.33 ± 0.08	0.021 ± 0.003	–
CN^-	2083	2.5 ± 0.4	10 ± 1	–	0.59 ± 0.04	0.41 ± 0.06	–	0.10 ± 0.03
CN bleach	2145	2.5 ± 0.5	10 ± 1	–	0.58 ± 0.06	0.42 ± 0.08	–	–1.46 ± 0.04

[a] Amplitudes normalized such that $\Sigma_i A_i = 1$. [b] A constant offset replaced A_3 for the bleach since it goes negative.

SIII. Kinetic Model (Scheme 1)

As discussed in the article, the model consists of ten coupled differential equations each of which describes the time-evolution of the concentration of one of the ten species in Scheme 1 (Figure S2). Both stimulated absorption and emission during the duration of the pump pulse are accounted for with forward- (k_i) and back- (k_{-i}) electron transfer rates. It is assumed that $k_i = k_{-i}$ and that each kinetic step is a first-order process.

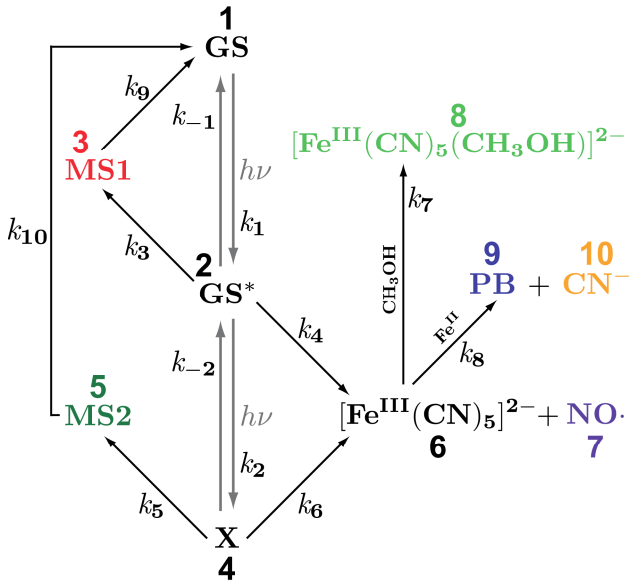

Figure S3. Scheme 1, as presented in the Article, including numbered labels on each of the species.

The set of differential equations in shown in Eqns. 3, where each species has been labeled with a number from 1–10. In the equations below, $k_{-1} = k_1$ and $k_{-2} = k_2$.

$$
\begin{aligned}
\dot{c}_1 &= k_1 c_2(t) - k_1 c_1(t) + k_9 c_3(t) + k_{10} c_5(t) \\
\dot{c}_2 &= k_1 c_1(t) - k_1 c_2(t) - k_2 c_2(t) + k_2 c_4(t) - k_3 c_2(t) - k_4 c_2(t) \\
\dot{c}_3 &= k_3 c_2(t) - k_9 c_3(t) \\
\dot{c}_4 &= k_2 c_2(t) - k_2 c_4(t) - k_5 c_4(t) - k_6 c_4(t) \\
\dot{c}_5 &= k_5 c_4(t) - k_{10} c_5(t) \\
\dot{c}_6 &= k_4 c_2(t) + k_6 c_4(t) - k_7 c_6(t) - k_8 c_6(t) \\
\dot{c}_7 &= k_4 c_2(t) + k_6 c_4(t) \\
\dot{c}_8 &= k_7 c_6(t) \\
\dot{c}_9 &= k_8 c_6(t) \\
\dot{c}_{10} &= k_8 c_6(t)
\end{aligned}
\tag{3}
$$

The solution of the model is obtained by the following procedure. First, Equation 3 is solved numerically with an initial guess of the rate constants ($k_9 = k_{10} = 1/110$ ns^{-1}) and the initial conditions at t = 2 ps (Table S4). This time is used to avoid pulse overlap effects in the experimental data. This solution is evaluated at the experimental time points and then subtracted from the solvent-subtracted experimental data (in units of mM). The eight rate constants are iteratively changed within their selected bounds (Tab. S4) using a nonlinear least-squares fitting routine to minimize the difference between experiment and model. Once the solution is found, Equation 3 is solved from t = 0 – 520 ps with the initial condition that $c_1(0) = 1$ (i.e. only the GS is populated before the pump pulse arrives at the sample).

Table S4. Model fitting parameters. The fit bounds for species 3–6 are based on the 300 fs time scale found for the formation of MS2 in the solid state.[4] The concentration at 2 ps is normalized to a sum of 1.

Species, i	τ_i (ps)	Fit Bounds (ps)	c_i (t = 2 ps) (Norm.)
1	0.010	[0.010, 0.020]	0.002
2	0.015	[0.010, 0.020]	0.008
3	0.30	[0.28, 0.32]	0.05
4	0.30	[0.28, 0.32]	0.01
5	0.30	[0.28, 0.32]	0.05
6	0.30	[0.28, 0.32]	0.44
7	130	[20, 500]	0.44
8	320	[20, 1000]	0
9	110000	–	0
10	110000	–	0

SIV. Molar Absorptivity Calculations

A. Quantum yield

The total photoexcitation yield was calculated by taking a ratio of the total integrated bleach area (Figs. 4a and S1) to the integrated area of the FTIR spectrum (Fig. 2) where self-absorption of the NO bleach was not included in the Gaussian fit.

Quantum yields of transient photoproducts were calculated using a ratio of the transient integrated area to that of the total bleach area. This was then multiplied by the total photoexcitation yield to give the final quantum yield. For transients that have molar absorptivities close to that of the parent species ($[Fe^{III}(CN)_5(CH_3OH)]^{2-}$, Prussian blue), transient concentrations can be obtained by multiplying the total quantum yield by the initial concentration (120 mM). For the other transient species (MS1, MS2, NO·, CN^-), molar absorptivities need to be calculated. Transient concentrations of all species (at t = 294 ps) can be calculated. Finally, transient quantum yields relative to $[Fe^{III}(CN)_5(CH_3OH)]^{2-}$ were calculated and factored into the total photoexcitation yield. The sum of the transient quantum yields is 1.93 ± 0.06%.

B. Integrated molar absorptivity

We report integrated molar absorptivities ($\varepsilon = \int \varepsilon_\nu d\nu$) of the NO stretch for the NO radical, MS1 and MS2. Since it is very difficult to obtain accurate cross-section information for these species, this information may prove to be useful in a variety of fields. The values were calculated by integrating the area under each of the transient species and dividing that area by the total bleach area where differences in sample concentrations for the CN region and NO region data were accounted for.

Simply taking the ratio of areas assumes that the molar absorptivity of the transient is the same as that of the parent species, which is accurate for $[Fe^{III}(CN)_5(CH_3OH)]^{2-}$ but not for NO· and CN^-. The concentration (at t = 294 ps) of $[Fe^{III}(CN)_5(CH_3OH)]^{2-}$ generated was ~1.2 mM. If we make the assumption that every NO photodissociation event leads to one solvent-associated species, then $c_{FeIII} = c_{NO\cdot}$. This gives enough information to calculate $\varepsilon_{NO}(NO\cdot) = 1.7 \times 10^2\ M^{-1}\ cm^{-2}$.

We estimate the molar absorptivities of the linkage isomers by taking the ratio of oscillator strengths of GS, MS1 and MS2 calculated using Gaussian 03[5] at the BP86 level

of theory[6] with 6-31G(d)[7] for iron and 6-311+G(3df)[8] for all other atoms. All calculations were performed using the polarizability continuum model with a methanol dielectric.[9] This allows the calculation of the transient concentration of the linkage isomers. The spectrum at t = 294 ps (y-axis converted to concentration) can then be fit to Gaussians to afford the area under the curve. The FTIR spectrum of SNP in methanol reveals $\varepsilon_{NO}(GS) = 3.3 \times 10^4$ M^{-1} cm^{-2}, from which we calculate $\varepsilon_{NO}(MS1) = 4.4 \times 10^4$ M^{-1} cm^{-2} and $\varepsilon_{NO}(MS2) = 2.0 \times 10^4$ M^{-1} cm^{-2}. Note that the error bars reported in the manuscript are derived from the error in the Gaussian fit of the experimental spectra.

References

(1) Sando, G.; Zhong, Q.; Owrutsky, J. C. *J. Chem. Phys.* **2004**, *121*, 2158.
(2) Bertie, J.; Zhang, S. *J. Mol. Struct.* **1997**, *413*, 333.
(3) Deoliveira, M. G.; Langley, G. J.; Rest, A. J. *J. Chem. Soc., Dalton Trans.* **1995**, 2013.
(4) Schaniel, D.; Nicoul, M; Woike, T. *Phys. Chem. Chem. Phys.* **2010**, *12*, 9029.
(5) Gaussian 03, Revision C.02, M. J. Frisch, G. W. Trucks, H. B. Schlegel, G. E. Scuseria, M. A. Robb, J. R. Cheeseman, J. A. Montgomery, Jr., T. Vreven, K. N. Kudin, J. C. Burant, J. M. Millam, S. S. Iyengar, J. Tomasi, V. Barone, B. Mennucci, M. Cossi, G. Scalmani, N. Rega, G. A. Petersson, H. Nakatsuji, M. Hada, M. Ehara, K. Toyota, R. Fukuda, J. Hasegawa, M. Ishida, T. Nakajima, Y. Honda, O. Kitao, H. Nakai, M. Klene, X. Li, J. E. Knox, H. P. Hratchian, J. B. Cross, V. Bakken, C. Adamo, J. Jaramillo, R. Gomperts, R. E. Stratmann, O. Yazyev, A. J. Austin, R. Cammi, C. Pomelli, J. W. Ochterski, P. Y. Ayala, K. Morokuma, G. A. Voth, P. Salvador, J. J. Dannenberg, V. G. Zakrzewski, S. Dapprich, A. D. Daniels, M. C. Strain, O. Farkas, D. K. Malick, A. D. Rabuck, K. Raghavachari, J. B. Foresman, J. V. Ortiz, Q. Cui, A. G. Baboul, S. Clifford, J. Cioslowski, B. B. Stefanov, G. Liu, A. Liashenko, P. Piskorz, I. Komaromi, R. L. Martin, D. J. Fox, T. Keith, M. A. Al-Laham, C. Y. Peng, A. Nanayakkara, M. Challacombe, P. M. W. Gill, B. Johnson, W. Chen, M. W. Wong, C. Gonzalez, and J. A. Pople, Gaussian, Inc., Wallingford CT, 2004.
(6) Becke, A. D. *Phys. Rev. A* **1988**, *38*, 3098.; Perdew, J. P. *Phys. Rev. B* **1986**, *33*, 8822.
(7) Rassolov, V.; Pople, J. A.; Ratner, M. A.; Windus, T. L. *J. Chem. Phys.* **1998**, *109*, 1223.
(8) Krishnan, R.; Binkley, J. S.; Seeger, R.; Pople, J. A. *J. Chem. Phys.* **1980**, *72*, 650.
(9) Tomasi, J.; Mennucci, B.; Cammi, R. *Chem. Rev.* **2005**, *105*, 2999.